THE JOURNAL OF BIOLOGICAL CHEMISTRY VOL. 281, NO. 5, pp. 2960–2968, February 3, 2006

Crystal Structure of a Viral FLIP

*INSIGHTS INTO FLIP-MEDIATED INHIBITION OF DEATH RECEPTOR SIGNALING**

Received for publication, October 12, 2005, and in revised form, November 16, 2005 Published, JBC Papers in Press, November 29, 2005, DOI 10.1074/jbc.M511074200

Feng-Yen Li, Philip D. Jeffrey, Jong W. Yu, and Yigong Shi[1]

From the Department of Molecular Biology, Princeton University, Lewis Thomas Laboratory, Princeton, New Jersey 08544

Death receptor signaling is initiated by the assembly of the death-inducing signaling complex, which culminates in the activation of the initiator caspase, either caspase-8 or caspase-10. A family of viral and cellular proteins, known as FLIP, plays an essential role in the regulation of death receptor signaling. Viral FLIP (v-FLIP) and short cellular FLIP (c-FLIP$_S$) inhibit apoptosis by interfering with death receptor signaling. The structure and mechanisms of v-FLIP and c-FLIP$_S$ remain largely unknown. Here we report a high resolution crystal structure of MC159, a v-FLIP derived from the molluscum contagiosum virus, which is a member of the human poxvirus family. Unexpectedly, the two tandem death effector domains (DEDs) of MC159 rigidly associate with each other through a hydrophobic interface. Structure-based sequence analysis suggests that this interface is conserved in the tandem DEDs from other v-FLIP, c-FLIP$_S$, and caspase-8 and -10. Strikingly, the overall packing arrangement between the two DEDs of MC159 resembles that between the caspase recruitment domains of Apaf-1 and caspase-9. In addition, each DED of MC159 contains a highly conserved binding motif on the surface, to which loss-of-function mutations in MC159 map. These observations, in conjunction with published evidence, reveal significant insights into the function of v-FLIP and suggest a mechanism by which v-FLIP and c-FLIP$_S$ inhibit death receptor signaling.

Apoptosis plays a central role in the development and homeostasis of metazoans (1–5). Inappropriate regulation of apoptosis contributes to a number of human pathologies, including cancer, autoimmune diseases, and neurodegenerative disorders (6–10). The pathways of apoptosis are evolutionarily conserved, culminating in the activation of death proteases, known as caspases (named after cysteine protease with Asp substrate specificity) (11, 12).

In mammalian cells, apoptosis manifests in two forms, intrinsic and extrinsic, which are triggered by cell death stimuli from intra- and extracellular environments, respectively. The extracellular death stimuli, such as the Fas/CD95 ligand, directly activate the death receptors through ligand-induced assembly of a death-inducing signaling complex (DISC)[2] at the plasma membrane (13, 14). The assembly of DISC results in the activation of caspase-8, which subsequently activates the effector caspases, caspase-3 and -7 (11).

The death receptor family comprises at least eight members, in which the TNFR1, Fas, and TRAIL receptors have been shown to activate apoptosis for immune system functions such as surveillance and elimination of virally infected or cancerous cells (15). The activated death ligands are homo-trimeric and thus induce oligomerization of the death receptors upon binding. The death receptors subsequently recruit the adaptor protein FADD (or TRADD for TNFR1) through direct interaction between a death domain (DD) present in both proteins (16–18). FADD, in turn, uses its death effector domain (DED) to interact with the N-terminal tandem DEDs of procaspase-8 or procaspase-10, thereby linking these initiator caspases to the activated death receptors within the DISC (19–21). Thus the assembly of DISC relies on homotypic DD and DED interactions and effectively facilitates the activation of initiator caspases.

To evade the host immune response, a number of viruses express distinct families of inhibitory proteins to suppress apoptosis and to promote their replication and survival in host cells (22). One important family of such proteins is the viral FLICE-inhibitory proteins (v-FLIPs), which were initially identified in molluscum contagiosum virus and in several γ-herpesviruses (22). v-FLIPs have been shown to block the activation of the death receptors at the level of DISC assembly (22). Some of the representative v-FLIP proteins include molluscum contagiosum virus MC159, equine herpesvirus-2 E8, herpesvirus saimiri ORF16, bovine herpesvirus-4 E2, and Kaposi's sarcoma associated herpesvirus (KSHV/HHV8) K13 (23–27). The hallmark of all v-FLIP proteins is two DED domains in tandem, which are also present in the prodomains of caspase-8 and caspase-10.

The presence of DEDs in v-FLIP immediately suggests potential interaction with FADD and caspase-8. Indeed, the DEDs of MC159 and E8 have been shown to interact with the DED of FADD and the prodomain of caspase-8 (23–26, 28). Through homotypic DED interactions, the v-FLIPs are thought to hinder efficient recruitment and subsequent activation of caspase-8 at the death receptors. Long and short cellular homologues of the v-FLIP have also been identified as c-FLIP$_L$ and c-FLIP$_S$, respectively (22). In addition to the tandem DEDs, c-FLIP$_L$ contains a caspase-like domain. For both c-FLIP$_S$ and c-FLIP$_L$, their tandem DEDs appear to antagonize death receptor signaling in the same manner when expressed at high levels (24, 29–31, 33–36).

Although the DED-containing proteins are known to control apoptosis from death receptors, the underlying mechanisms remain largely unknown. This is in part due to the technical difficulty in working with membrane-associated protein complexes. As a consequence, there is a lack of comprehensive structural information on the relevant proteins and protein complexes. At present, we only have limited structural information on the isolated DED of FADD (37) and Pea-15 (38), and the DD of Fas (39) and FADD (40, 41). All structures conform to a common fold comprising six antiparallel α-helices, which is also shared by caspase recruitment domain (CARD) (42).

* This work was supported by grants from the National Institutes of Health. The costs of publication of this article were defrayed in part by the payment of page charges. This article must therefore be hereby marked "*advertisement*" in accordance with 18 U.S.C. Section 1734 solely to indicate this fact.

The atomic coordinates and structure factors (code 2F1S) have been deposited in the Protein Data Bank, Research Collaboratory for Structural Bioinformatics, Rutgers University, New Brunswick, NJ (http://www.rcsb.org/).

[1] To whom correspondence should be addressed: Dept. of Molecular Biology, Princeton University, Washington Road, Princeton, NJ 08544. Tel.: 609-258-6071; Fax: 609-258-6730; E-mail: yshi@molbio.princeton.edu.

[2] The abbreviations used are: DISC, death-inducing signaling complex; TNFR1, tumor necrosis factor receptor 1; TRAIL, TNF-related apoptosis-inducing ligand; DD, death domain; DED, death effector domain; CARD, caspase recruitment domain; SeMet, seleno-methionine; MAD, multiwavelength anomalous dispersion; r.m.s.d., root-mean-square deviation.

TABLE 1

Statistics of crystallographic analysis

R-sym = $S_h S_i |I_{h,i} - I_h| / S_h S_i I_{h,I}$, where I_h is the mean intensity of the *i* observations of symmetry related reflections of *h*. *R*-sym for SeMet MAD data includes anomalous signal. The number of reflections and completeness refer to the working set only, the free set was an additional ~4.8% of the data. $R = \Sigma |F_{obs} - F_{calc}| / \Sigma F_{obs}$, where $F_{obs} = F_p$, and F_{calc} is the calculated protein structure factor from the atomic model (R_{free} was calculated with 5% of the reflections). r.m.s.d. in bond lengths and angles are the deviations from ideal values, and the r.m.s.d. in *B*-factors is calculated between bonded atoms.

Data collection	Native	SeMet			
		Peak	Inflection	High remote	Low remote
Wavelength (Å)	0.9795	0.9790	0.9794	0.9641	0.9800
Resolution (Å)	50–1.4	50–1.75	50–1.75	50–1.75	50–1.5
Total observations	153,552	102,394	102,687	102,277	96,746
Unique reflections	33,495	17,764	17,717	17,708	28,066
***R*-sym (%)**	3.6	7.3	6.8	6.8	4.6
Completeness (%)	98.0	99.3	98.9	98.8	99.4
Refinement					
Resolution (Å)	50–1.4				50–1.5
Reflections ($\|F\| > 0$)	31,044				26267
Completeness (%)	91.2				93.4
R-factor (%)	20.6				19.5
R-free (%)	23.6				21.7
No. atoms	1376				1376
No. waters	174				175
r.m.s.d. bond lengths	0.014				0.014
r.m.s.d. bond angles	1.62				1.64
r.m.s.d. *B*-factors	2.80				2.61
Ramachandran plot					
Most favored (%)	95.1				98.3

To gain insights into the mechanism by which v-FLIP inhibits death receptor signaling, we determined the crystal structure of MC159 at 1.4-Å resolution. This structure reveals a number of unexpected findings that significantly assist the deciphering of mechanisms by which v-FLIP and c-FLIP$_S$ function.

EXPERIMENTAL PROCEDURES

Protein Purification—A cDNA fragment encoding MC159-(1–183) was subcloned into pGEX-2T (Amersham Biosciences) and transformed into BL21(DE3) *Escherichia coli*-competent cells. Cells were grown to an A_{600} of 1.0 at 37 °C before induction with 0.5 mM isopropyl 1-thio-β-D-galactopyranoside at 23 °C overnight. The N-terminal glutathione *S*-transferase-tagged MC159 protein was purified as previously described (43). The preparation of the seleno-methionine (SeMet)-substituted MC159 (residues 1–183) was as described (44).

Crystallization and Data Collection—Similar rod-shaped crystals of native and SeMet MC159 protein (residues 1–183) were grown overnight at room temperature using the hanging drop vapor diffusion method. The best SeMet crystals were generated by streak seeding under the condition of 0.2 M sodium acetate, 0.1 M Tris hydrochloride, pH 8.5, and 14% polyethylene glycol 3350, with 0.5 μl of 1 M ammonium sulfate additive. Data were collected at the X25 beam line of Brookhaven National Synchrotron Light Source. MAD data were collected at the Selenium K edge to a maximum resolution of 1.5 Å. A native data set was collected at 1.4 Å using a crystal grown at the same conditions as the SeMet crystals except 16% (w/v) polyethylene glycol 3350 was used. Both crystals were cryoprotected in a buffer containing 0.2 M sodium acetate, 0.1 M Tris hydrochloride, pH 8.5, 18% w/v polyethylene glycol 3350, 0.15 M ammonium acetate, and 10% glycerol. The crystals had a primitive orthorhombic space group with unit cell dimensions of $a = 35$ Å, $b = 63$ Å, $c = 76$ Å, and $a = b = c = 90°$. Unit cell dimensions were consistent with one molecule per asymmetric unit.

Structure Determination—For the MAD experiments, data were processed using the HKL suite of programs (45). Systematic absences for reflections of classes h00, 0k0, and 00l in both the SeMet and native data strongly indicated that the space group was $P2_12_12_1$. The SHELX suite of programs (46) was used to extract experimental phase information. The MAD data were prepared for structure determination with SHELXC, and four out of five possible selenium atom sites were found by SHELXD. The contrast in the solvent-flattened electron density maps in SHELXE unambiguously distinguished between the correct and inverted heavy atom locations (contrast of 0.445 and 0.268, respectively). The electron density map, generated from SHELXE, was clearly interpretable, and given the high resolution of the MAD data, the structure was automatically build from solvent-flattened MAD phases calculated to 1.5-Å resolution using the program ARP/wARP (47). Further manual building using the program O (48) and refinement using the program CNS (49) completed the structure. The final atomic model of MC159, refined to 1.4-Å resolution, contains residues 7–183. There is no electron density for residues 1–6, and we presume that these residues are flexible and disordered in the crystals.

RESULTS AND DISCUSSION

Overall Structure of the Tandem DEDs of MC159—The full-length MC159 protein (residues 1–241) consists of two tandem DEDs and a C-terminal extension. Both sequence analysis and limited proteolysis indicated that the C-terminal extension of MC159 is flexible and disordered in solution. Because flexible sequences may impede crystallization, we generated and purified a truncated version (residues 1–183) of MC159, which contains the two tandem DEDs but lacks the C-terminal extension. We crystallized the truncated MC159 and determined its structure using multiwavelength anomalous dispersion (MAD). The atomic model was refined to 1.4-Å resolution (Table 1).

The truncated MC159 adopts a dumbbell-shaped structure, with the two DEDs at two opposing ends (Fig. 1, *A* and *B*). The two DED domains can be superimposed onto each other with a root-mean-squared deviation (r.m.s.d.) of 1.78 Å over 60 aligned Cα atoms (Fig. 1*C*). The first DED domain (DED1, residues 7–78) of MC159 only contains five α-helices and represents a departure from the canonical death motif fold (Fig. 1*A*). Consequently, DED1 of MC159 is superimposed with the DED of FADD (37) with an r.m.s.d. of 1.84 Å over only 45 aligned Cα atoms. These 45 aligned amino acids come from helices α1a, α2a, α5a, and α6a

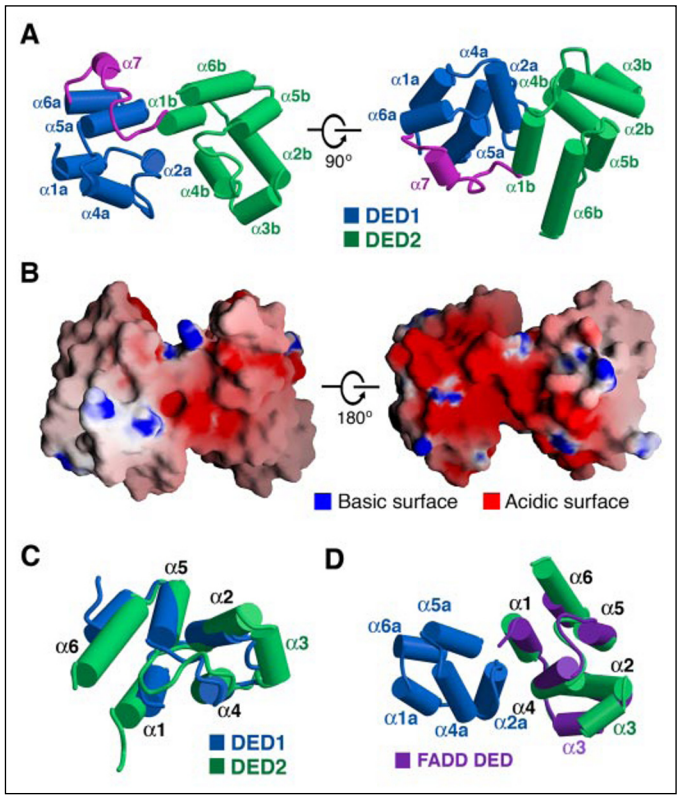

FIGURE 1. **Overall structure of MC159 (residues 7–183).** *A*, schematic representation of the structure of the MC159 protein (residues 7–183). The first and second DED domains are colored *blue* and *green*, respectively. The linker region is colored *magenta*. This coloring scheme is preserved in all subsequent figures. *B*, surface representation of the MC159 structure. The acidic and basic surfaces are identified by *red* and *blue colors*, respectively. MC159 in the *right panel* is shown in the same orientation as that in the *right panel* of *panel A*. *C*, structure overlay of the two DED domains of MC159. The third helix in DED1 is reduced to a surface loop. *D*, structure overlay of FADD DED with DED2 of MC159. FADD DED is shown in *purple*. All figures were prepared using MOLSCRIPT (55) and GRASP (32).

in DED1. Compared with the DED of FADD (37) and the second DED (DED2, residues 93–183) of MC159, the third α-helix is reduced to a rigid loop in DED1 of MC159. Sequence analysis suggests that this structural feature might be unique to MC159, because, compared with FADD and other proteins, MC159 lacks a few conserved residues in the region that corresponds to the α3a helix (Fig. 2). In contrast, the second DED domain (DED2, residues 93–183) of MC159 can be superimposed with the DED of FADD with an r.m.s.d. of 1.57 Å over 80 aligned Cα atoms, which cover all six α-helices and most of the intervening loop sequences (Fig. 1*D*).

DED1 and DED2 are connected by a stretch of 14 amino acids (residues 79–92), which form a short helix α7 and two surface loops. Unexpectedly, the two DED domains of MC159 rigidly associate with each other through a hydrophobic interface, involving ~1450 Å^2 of buried surface area. The close stacking between the two DED domains of MC159 creates a deep surface groove that encircles the molecule (Fig. 1*B*). This surface groove is lined with a number of acidic amino acids that give rise to a highly negatively charged surface. In contrast, the two opposing ends of the MC159 structure are less charged and contain a number of hydrophobic residues.

Conserved Interactions at the DED1-DED2 Interface—Of the three classes of signaling motifs in apoptosis, only DED is known to occur in tandem, and the tandem DEDs are present in all known v-FLIPs, c-FLIP$_L$, c-FLIP$_S$, caspase-8, and caspase-10 (Fig. 2). One important finding from the structure of MC159 is the unexpected revelation that the two tandem DED domains pack closely against each other through a large hydrophobic interface. At this interface, α2a in DED1 plays a dominant role by binding to α1b and α4b of DED2 (Figs. 2 and 3*A*). Another helix from DED1, α5a, also contributes to this interface by making additional interactions at the periphery (Fig. 3*A*).

At the center of the interface, Phe-30 and Leu-31, both from α2a in DED1, make multiple van der Waals contacts to a complementary hydrophobic surface in DED2, formed by Val-101, Val-137, and Leu-141 and the aliphatic portion of side chains of Arg-97 and Lys-98 (Fig. 3*A*). At the periphery, Leu-27 and Val-66 in DED1 make additional interactions with hydrophobic residues in DED2. These hydrophobic interactions are further buttressed by five inter-domain hydrogen bonds (Fig. 3*A*). In particular, Asp-34 in DED1 accepts a pair of charge-stabilized hydrogen bonds from Arg-97 in DED2.

Structural and sequence analysis indicates that the interactions at the DED1-DED2 interface are highly conserved among all proteins that contain tandem DED domains (Figs. 2 and 3*A*). Among the residues that mediate interactions at the center of the interface, Phe-30, Leu-31, Arg-97, Val-137, and Leu-141, are either preserved or replaced by similar residues in all proteins that contain tandem DED domains (Fig. 2). Moreover, the hydrogen bonds between Asp-34 and Arg-97 are also predicted to be conserved in a majority of these proteins (Fig. 2). This analysis strongly suggests that the rigid structure of MC159 and the interface determinants between the tandem DEDs are representative of v-FLIPs, c-FLIP, caspase-8, and caspase-10.

Similarity with CARD-CARD Interactions—Because there is no prior structural information on any DED·DED complex or on any tandem DED-containing protein, we initially assumed that the packing arrangement between the two DED domains of MC159 might represent a novel arrangement. To confirm this assumption, we used the atomic coordinates of the MC159 protein to search the protein data base using the program DALI (50) as well as our own automated homology search program (P. D. J.). To our surprise, the packing interactions between the two DEDs of MC159 were found to be significantly homologous to those between the CARD domains of Apaf-1 and caspase-9 (51) (Fig. 3*B*), with an r.m.s.d. of 1.8 Å over 85 aligned Cα atoms in both domains. The relative domain orientation and the interface are both very similar. In both cases, the α2 helix in DED1 of MC159 or in Apaf-1 CARD plays a dominant role in binding to helices α1 and α4 in DED2 of MC159 or in caspase-9 CARD (51). The inter-domain hydrogen bonds from Asp-34 of DED1 to Arg-97 of DED2 (Fig. 3*A*) are also reminiscent of the CARD-CARD interactions, where acidic residues from Apaf-1 hydrogen bond to basic residues in caspase-9 (51). This analysis indicates that, despite a lack of apparent sequence homology, the DED1-DED2 interface observed in MC159 is very similar to the CARD-CARD interface between Apaf-1 and caspase-9. This observation further suggests that the tandem DED domains in FLIP and caspases might have arisen from gene transfer (from another interacting protein) rather than gene duplication (within the same protein).

Classification of Mutations in MC159—As one of the first v-FLIP proteins to be identified, MC159 had been subjected to intense investigation. In particular, an extensive alanine-scanning mutagenesis was performed on MC159 to identify important amino acids that are critical for its anti-apoptotic function *in vivo* (52). This effort led to the identification of a comprehensive set of amino acids in both DEDs that are required to protect HeLa and Jurkat cells from apoptosis induced by TNFR1, Fas, and TRAIL receptors (52). In conjunction with the structure, the mutagenesis information gives us an unprecedented opportunity to map the critical residues onto the surface of MC159 and to further identify critical surface motifs necessary for the anti-apoptotic function of MC159.

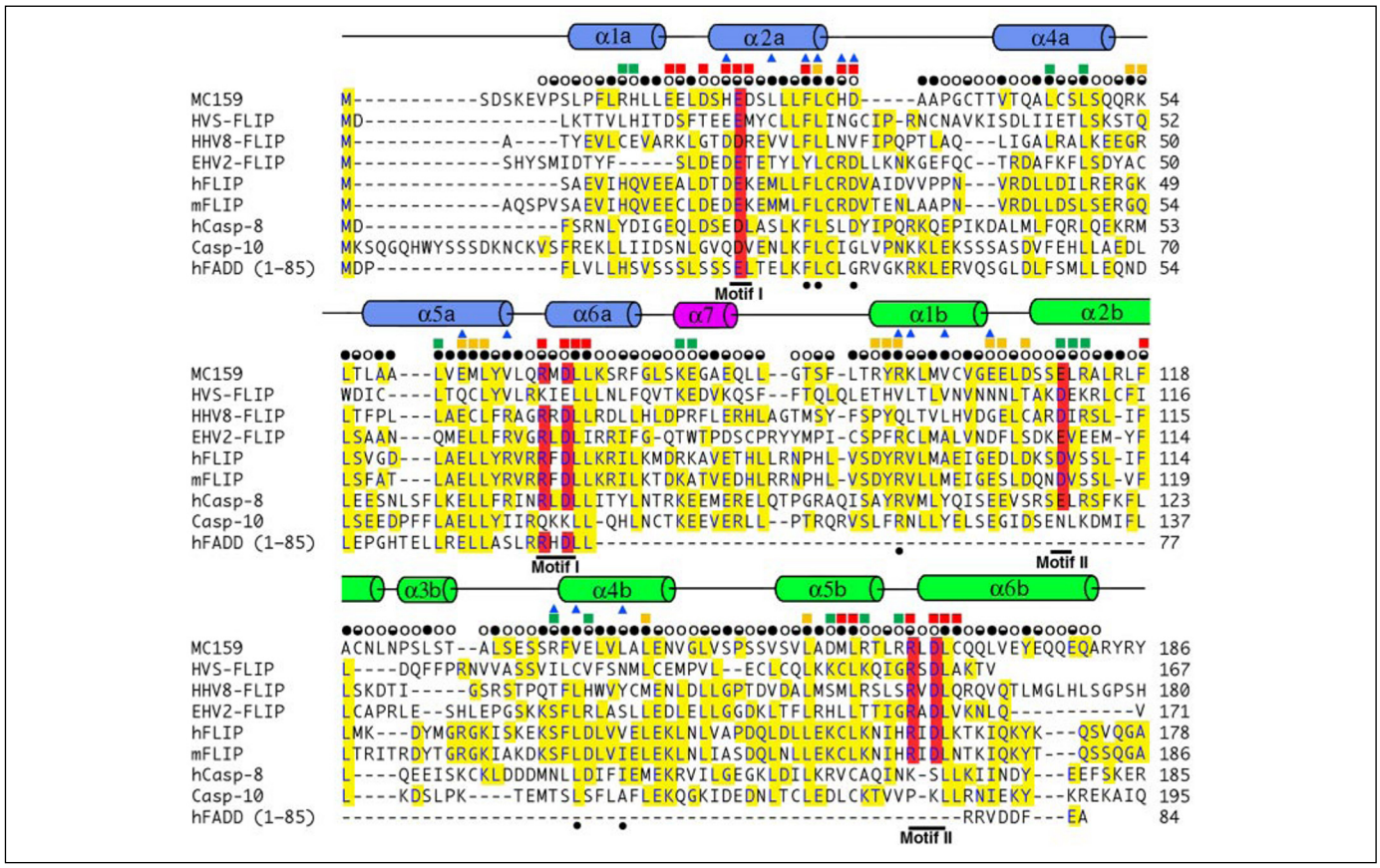

FIGURE 2. **Structure-based sequence alignment of the DED regions from v-FLIPs, c-FLIP, FADD, and caspase-8 and caspase-10.** Secondary structural elements are indicated above the MC159 sequences. Conserved residues are highlighted in *yellow*. The conserved binding elements on the surface of DED1 and DED2 are indicated, with the residues under *red background*. Residues that contribute to the interactions between DED1 and DED2 are identified with *blue triangles*. The highly conserved residues that play important stabilizing roles at the DED interface are identified by *black dots* underneath the sequences. The effect of alanine-scanning mutagenesis is indicated by *colored squares* above the sequences: *red*, loss-of-function; *yellow*, partial loss-of-function; *green*, no effect (52). Amino acid residues that are $>$ 40% solvent-exposed, 10–40% solvent-exposed, and $<$10% solvent-exposed are indicated by *open*, *half-filled*, and *filled circles* above the sequences, respectively.

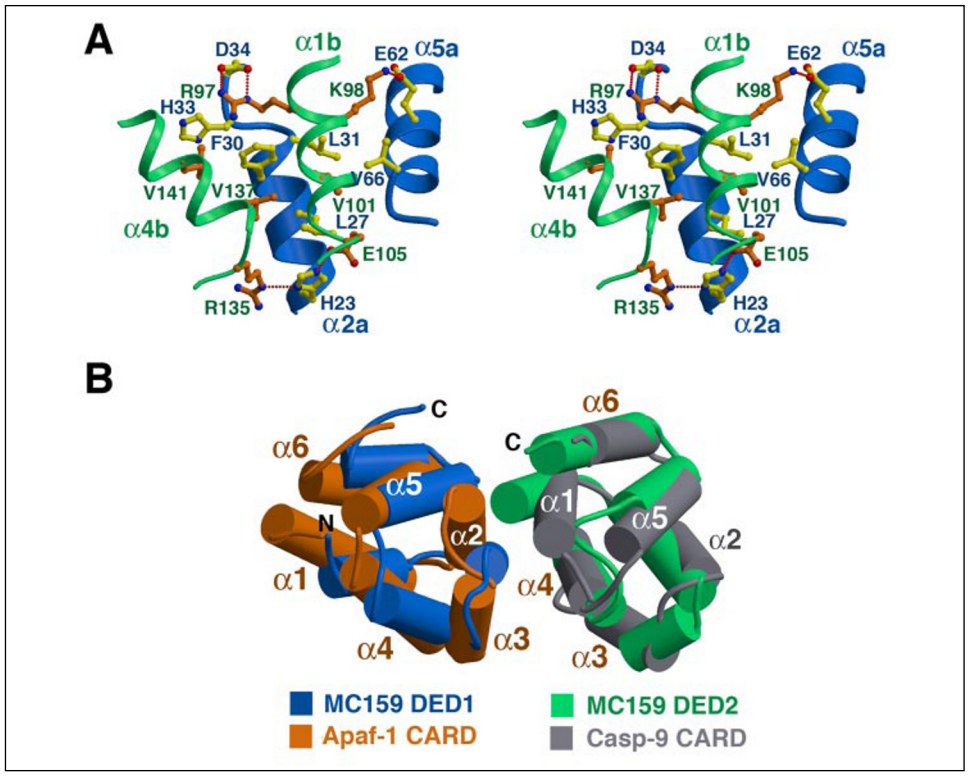

FIGURE 3. **The interface between the two tandem DED domains in MC159 resembles that of the CARD·CARD complex between Apaf-1 and caspase-9.** *A*, a stereo view of the interactions at the DED1-DED2 interface. Hydrogen bonds are represented by *red dashed lines*. *B*, the relative orientation between DED1 and DED2 of MC159 resembles that between the CARD domains of Apaf-1 and caspase-9. The structure of MC159 is aligned with that of the CARD·CARD complex between Apaf-1 (*orange*) and caspase-9 (*gray*) (51).

TABLE 2

Structural analysis of alanine scanning mutagenesis data on MC159

Mutations characterized together by a single mutant are listed within the same group (Garvey *et al.* (52)). The degree of the loss of function for the MC159 mutant is denoted by the footnotes *a*–*c* next to the mutation.

Mutation	Mutant	Solvent accessibility	Predicted effect	Location on structure	Special location
R14A[a]	1	Exposed	Non-structural	DED1-α1a	
H15A[a]		Exposed	Non-structural	DED1-α1a	
E18A[b]	16	Exposed	Non-structural	DED1-α1a-α2a	
E19A[b]		Exposed	Non-structural	DED1-α1a-α2a	
D21A[b]		Exposed	Non-structural	DED1-α1a-α2a	
H23A[b]	2	Partially exposed	Non-structural	DED1-α2a	DED interface
E24A[b]		Partially exposed	Non-structural	DED1-α2a	DED interface
D25A[b]		Partially exposed	Non-structural	DED1-α2a	DED interface
F30A[b]	17	Buried	Structural	DED1-α2a	DED interface
L31A[b]	24	Buried	Structural	DED1-α2a	DED interface
H33A[b]	3	Partially exposed	Non-structural	DED1-α2a-α4a	DED interface
D34A[b]		Exposed	Non-structural	DED1-α2a-α4a	DED interface
L46A[a]	25	Buried	Structural	DED1-α4a	
L49A[a]	23	Buried	Structural	DED1-D1-α4a	
R53A[a]	4	Exposed	Non-structural	DED1-α4a-α5a	
K54A[a]		Partially exposed	Non-structural	DED1-α4a-α5a	
L60A[a]	30	Buried	Structural	DED1-α5a	
E62A[b]	5	Buried	Structural	DED1-α5a	DED interface
R69A[c]	6	Partially exposed	Non-structural	DED1-α5a-α6a	Binding motif I
D71A[c]		Exposed	Non-structural	DED1-α6a	Binding motif I
L72A[c]	21	Buried	Structural	DED1-α6a	
L73A[c]		Buried	Structural	DED1-α6a	
K81A[a]	7	Exposed	Non-structural	α7	Between DEDs
E82A[a]		Exposed	Non-structural	α7	Between DEDs
R95A[b]	8	Exposed	Non-structural	DED2-α1b	
Y96A[b]		Buried	Structural	DED2-α1b	
R97A[b]		Buried	Structural	DED2-α1b	DED interface
E105A[b]	9	Exposed	Non-structural	DED2-α1b-α2b	DED interface
E106A[b]		Exposed	Non-structural	DED2-α1b-α2b	
D108A[b]		Exposed	Non-structural	DED2-α1b-α2b	
E111A[a]	18	Partially exposed	Non-structural	DED2-α2b	
L112A[a]		Partially exposed	Non-structural	DED2-α2b	
R113A[a]		Exposed	Non-structural	DED2-α2b	
F118A[a]	19	Partially exposed	Non-structural	DED2-α2b	
R135A[a]	10	Partially exposed	Non-structural	DED2-α4b	
E138A[a]		Partially exposed	Non-structural	DED2-α4b	
L143A[a]	26	Buried	Structural	DED2-α4b	
L157A[a]	29	Partially exposed	Non-structural	DED2-α5b	
D159A[a]	11	Exposed	Non-structural	DED2-α5b	
M160A[a]	27	Buried	Structural	DED2-α5b	
L161A[a]		Buried	Structural	DED2-α5b	
R162A[a]	20	Exposed	Non-structural	DED2-α5b	
R165A[a]		Exposed	Non-structural	DED2-α5b-α6b	
R166A[c]	12	Partially exposed	Non-structural	DED2-α5b-α6b	Binding motif II
D168A[c]		Exposed	Non-structural	DED2-α6b	Binding motif II
L169A[a]	28	Buried	Structural	DED2-α6b	
C170A[a]		Buried	Structural	DED2-α6b	
E62A[b]	31	Buried	Structural	DED1-α5a	DED interface
D159A[b]	(5 + 11)	Exposed	Non-structural	DED2-α5b	
F30A[c]	32	Buried	Structural	DED1-α2a	DED interface
F118A[c]	(17 + 19)	Partially exposed	Non-structural	DED2-α2b	
E18A[c]	33	Exposed	Non-structural	DED1-α1a-α2a	
E19A[c]	(16 + 19)	Exposed	Non-structural	DED1-α1a-α2a	
D21A[c]		Exposed	Non-structural	DED1-α1a-α2a	
F118A[c]		Partially exposed	Non-structural	DED2-α2b	
E18A[c]	34	Exposed	Non-structural	DED1-α1a-α2a	
E19A[c]	(16 + 17)	Exposed	Non-structural	DED1-α1a-α2a	
D21A[c]		Exposed	Non-structural	DED1-α1a-α2a	
F30A[c]		Buried	Structural	DED1-α2a	DED interface
H23A[c]	35	Partially exposed	Non-structural	DED1-α2a	DED interface
E24A[c]	(2 + 3)	Partially exposed	Non-structural	DED1-α2a	DED interface
D25A[c]		Partially exposed	Non-structural	DED1-α2a	DED interface
H33A[c]		Partially exposed	Non-structural	DED1-α2a-α4a	DED interface
D34A[c]		Exposed	Non-structural	DED1-α2a-α4a	DED interface
R53A[b]	36	Exposed	Non-structural	DED1-α4a-α5a	
K54A[b]	(4 + 22)	Partially exposed	Non-structural	DED1-α4a-α5a	
M63A[b]		Buried	Structural	DED1-α5a	
L64A[b]		Buried	Structural	DED1-α5a	
K81A[b]	37	Exposed	Non-structural	α7	Between DEDs
E82A[b]	(7 + 8)	Exposed	Non-structural	α7	Between DEDs
R95A[b]		Exposed	Non-structural	DED2-α1b	
Y96A[b]		Buried	Structural	DED2-α1b	
R97A[b]		Buried	Structural	DED2-α1b	DED interface
L143A[b]	38	Buried	Structural	DED2-α4b	
L157A[b]	(26 + 29)	Partially exposed	Non-structural	DED2-α5b	
M160A[c]	39	Buried	Structural	DED2-α5b	
L161A[c]	(27 + 28)	Buried	Structural	DED2-α5b	
L169A[c]		Buried	Structural	DED2-α6b	

TABLE 2—*CONTINUED*

Mutation	Mutant	Solvent accessibility	Predicted effect	Location on structure	Special location
C170A[c]		Buried	Structural	DED2-α6b	
L28A[c]	40	Buried	Structural	DED1-α2a	
L29A[c]		Partiallyexposed	Non-structural	DED1-α2a	
L31A[c]		Buried	Structural	DED1-α2a	DEDinterface

[a] No loss (Garvey *et al.* (52)).
[b] Partial loss (52).
[c] Complete loss (52).

The mutations may disrupt the function of MC159 by two distinct possibilities: to destabilize the structure or to affect a functional surface that is required for binding to other protein(s). To differentiate between these two possibilities, we first examined the solvent accessibility of all residues that were targeted for alanine scanning mutagenesis (Fig. 2) and classified the mutations into two categories: structural or non-structural (Table 2). Then we correlated the classification with the *in vivo* phenotypes (Table 2) and mapped all mutations onto the surface of the MC159 structure (Fig. 4, *A* and *B*). As expected, some mutations affect residues that are deeply buried, such as mutant 5 (E62A), mutant 17 (F30A), mutant 21 (L72A/L73A), mutant 24 (L31A), and mutant 40 (L28A/L29A/L31) (Table 2). These mutations are likely to destabilize the structure of MC159, thus crippling its function. Interestingly, among these structural mutations, a significant portion map to the interface between DED1 and DED2 (Table 2), suggesting that distorting the relative orientation of the tandem DED domains may significantly compromise the function of MC159. For example, Phe-30 and Leu-31 are located in the center of the DED1-DED2 interface, whereas Glu-62 is involved in a hydrogen bond at the interface (Fig. 3*A*).

Identification of a Conserved Binding Element on DED—The mutations that affect solvent-exposed residues are unlikely to disrupt the structure and are expected to affect a functional surface that is required for binding to other protein(s). Thus these mutations are particularly informative. There are a number of such mutations (Table 2), which map primarily to four distinct surface patches, three on one face and one on the opposite face of the MC159 structure (Fig. 4, *A* and *B*, highlighted in *red*). Mutations of residues in these four surface patches were found to significantly compromise or abolish the anti-apoptosis function of MC159 (52). These surface patches are likely involved in binding to FADD, caspase-8, or other proteins. The presence of multiple binding elements on the surface of MC159 also suggests that MC159 might participate in a network of interactions involving at least two binding components.

The most prominent loss-of-function mutants of MC159 are mutant 6 (R69A/D71A) and mutant 12 (R166A/D168A), both of which affect exposed or partially exposed residues at the center of the prominent surface patches of motifs 1 and 2 (Table 2 and Fig. 4 (*B* and *C*)). Both Arg-69/Asp-71 and Arg-166/Asp-168 are located at the beginning of helix α6 in DED1 and DED2, respectively, and they are involved in identical interactions. Asp-71 in DED1 or Asp-168 in DED2 accepts a pair of charge-stabilized hydrogen bonds from Arg-69 in DED1 or Arg-166 in DED2, respectively. These interactions are further stabilized by a hydrogen bond from Glu-24 to Arg-71 in DED1 and Glu-111 to Arg-166 in DED2 (Fig. 4*C*). These observations suggest that the surface patch on each DED, defined by the Glu-Arg-Asp interactions, is likely to be a binding element for another protein. Importantly, sequence analysis indicates that this binding element is well conserved among all tandem DED containing proteins except caspase-10 (Fig. 2).

Models of v-FLIP Binding to FADD and Caspase-8—Viral FLIPs and c-FLIP are thought to antagonize apoptosis through interactions with FADD and caspase-8 (22), although the underlying mechanisms remain unclear. The structure of MC159 and the identification of candidate binding elements on MC159 allow us to propose working models to explain the function of v-FLIP and c-FLIP. This effort is greatly facilitated by the distinct scenario that there may be a very limited number of ways for the homotypic interaction motifs to interact with each other and with other binding proteins. At present, only two distinct modes of interaction among the homotypic interaction motifs have been documented in structural detail, as exemplified by the interactions between the DDs of Pelle and Tube (53) and between the CARDs of Apaf-1 and caspase-9 (51) (Fig. 5*A*). In this study, we demonstrate that, despite a lack of sequence homology, the relative binding arrangement between DED1 and DED2 of MC159 closely resembles that between the CARD domains of Apaf-1 and caspase-9 (Fig. 3*B*). In another study (38), the DED domain of PEA-15 was found to use a similar motif to recognize its binding protein as the DD domain of Tube. Strikingly, the same motif used by PEA-15 DED and by Tube DD, involving the beginning of helix α6 and helix α2, exactly maps to the conserved binding element (motifs 1 and 2) on both DEDs of MC159 and other tandem DED-containing proteins (Fig. 2). Thus we postulate that the conserved binding element on the DED of MC159 uses a similar binding mode to interact with FADD and caspase-8 as observed in the complex between Pelle and Tube (53).

On the basis of this assumption, we generated a number of hypothetical models describing how the DEDs of MC159, caspase-8, and FADD would assemble onto each other (Fig. 5*B*). In these models, MC159 uses the two conserved surface binding elements (motifs 1 and 2) to interact with the DEDs of caspase-8 and the DED of FADD, mimicking the binding mode observed in the Pelle·Tube complex. This arrangement naturally allows the DEDs of FADD and caspase-8 to interact with each other in a way similar to that of DED1 and DED2 of MC159, or the CARD domains of Apaf-1 and caspase-9. For one of these models (scenario 1), we used the exact Pelle·Tube DD interface to create a detailed three-dimensional view (Fig. 5*C*). Strikingly, the shape complementarity is excellent among MC159, FADD, and caspase-8, and there is no steric clash among any pair of molecules in these models. Importantly, loss-of-function mutations that affect amino acids on the surface of MC159 predominantly map to the interface between MC159 and caspase-8 or between MC159 and FADD (Fig. 5*C*). Thus these models provide a plausible explanation to the observed functional phenotypes. We further hypothesize that, by forming a ternary complex with FADD and caspase-8, MC159 disrupts the interactions between FADD and caspase-8 that are required for the appropriate activation of caspase-8 (Fig. 5*D*). Sequence conservation strongly suggests that the mechanism by which MC159 functions is likely to be conserved among other members of v-FLIP as well as c-FLIP.

It is worth noting that, in theory, each homotypic interaction motif (such as the DED of FADD) contains four putative surface regions that might be involved in the two known types of homotypic interactions (as exemplified by the DDs of Tube·Pelle and the CARDs of Apaf-1/Caspase-9). In scenario I of Fig. 5*B*, in which the DED1 and DED2 of FLIP are postulated to mimic Tube in binding to the corresponding DEDs of caspase-8 and FADD, only two surface regions are used for each DED of FLIP: one for binding to DED of

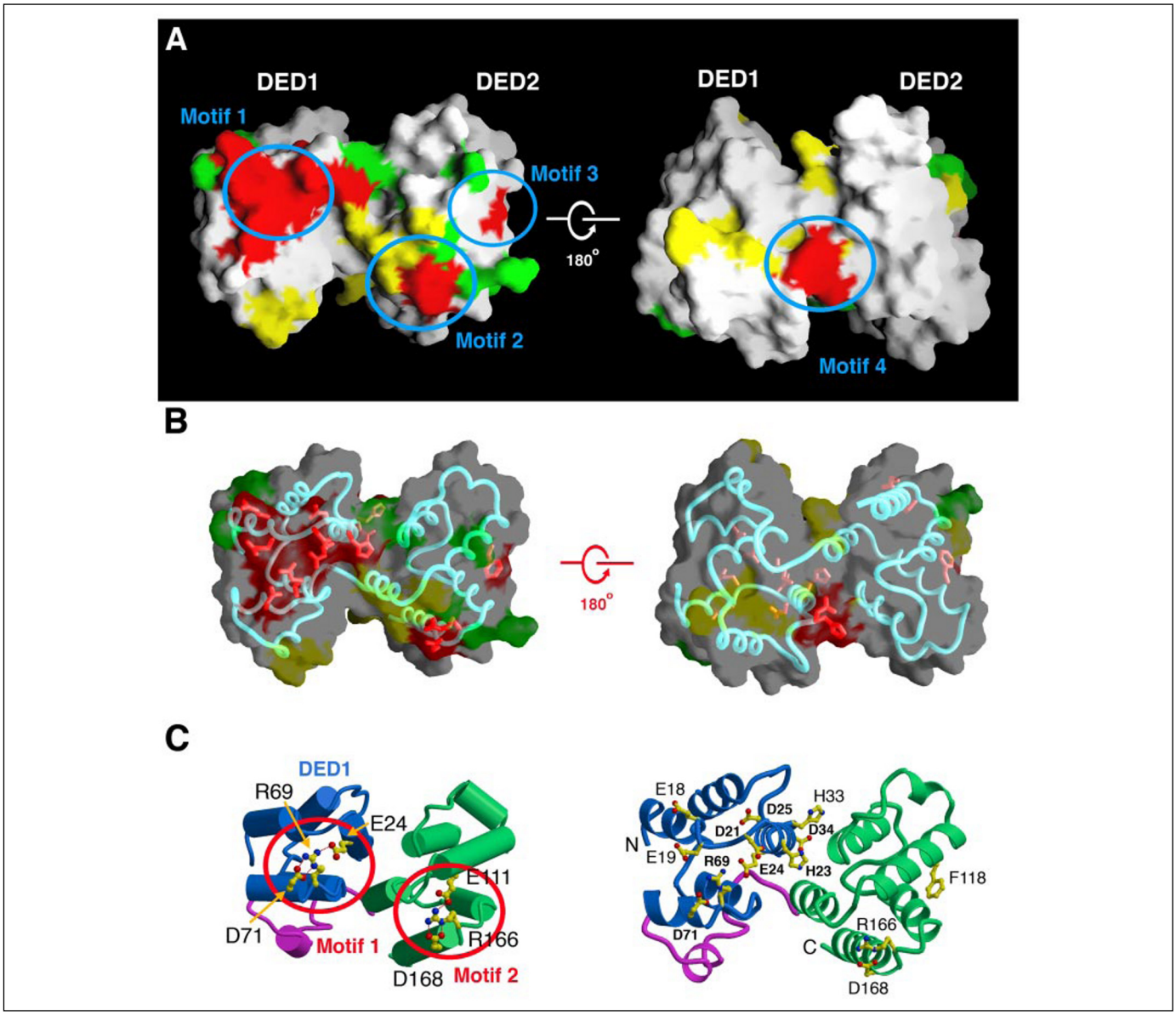

FIGURE 4. **Loss-of-function mutations in MC159 map to distinct surface patches on the structure.** *A*, mutations in MC159 map to four distinct surface patches on the structure. The structure of MC159 is shown in a *surface representation*. Residues that were targeted for alanine-scanning mutagenesis are mapped to the surface. Residues whose mutation contributed to loss-of-function, partial loss-of-function, and no loss-of-function in MC159 are colored *red*, *yellow*, and *green*, respectively. This analysis identified four surface motifs that represent potential binding elements for other proteins. *B*, locations of the residues whose mutation contributed to loss-of-function in MC159. The structure of MC159 is shown in a *transparent surface representation*, with the backbone shown in *cyan* and the affected residues shown in *red*. For the identity of these residues, please refer to the *right panel* in *C*, which is shown in the same orientation as the *left panel* in *B*. *C*, identification of a conserved binding element on the DED domains of MC159. Glu-24/Arg-69/Asp-71 in DED1 and Glu-111/Arg-166/Asp-168 in DED2 display an identical set of interactions and are highly conserved in the tandem DED-containing proteins.

caspase-8 or FADD and the other for intramolecular interaction with its neighboring DED. Hence the DED1 and DED2 of FLIP still have free surface regions that could bridge additional interactions. The presence of multiple interaction surface regions in the homotypic interaction motifs is consistent with the formation of death effector filament by the DEDs of caspase-8 and FADD, which correlated with apoptosis phenotype (54).

One important feature of these models is that the interactions among v-FLIP, FADD, and caspase-8 are cooperative, because multiple interfaces are involved (Fig. 5*B*). Supporting these models, we used recombinant proteins to show that MC159 or c-FLIP$_S$ forms a stable ternary complex with FADD and the tandem DED domains of caspase-8 (data not shown). The cooperative feature predicts that mild mutations of one interface may not be sufficient to abolish the association between MC159 and caspase-8 or FADD. However, such mutations may cause sufficient changes at the local surface area such that the relative orientation between MC159 and caspase-8 or FADD had been altered, which could no longer support MC159-mediated normal function (to suppress apoptosis). This could explain why some of the loss-of-function mutants of MC159 retained binding to caspase-8 and/or FADD (52).

Despite some supporting evidence, we recognize that these models are hypothetical and must be tested experimentally. In fact, the presence of multiple binding elements on the surface of MC159 makes any detailed model highly speculative in nature. Nonetheless, the identification of candidate binding elements on the surface of MC159 represents a concrete and important step toward future biochemical and cell biological characterization.

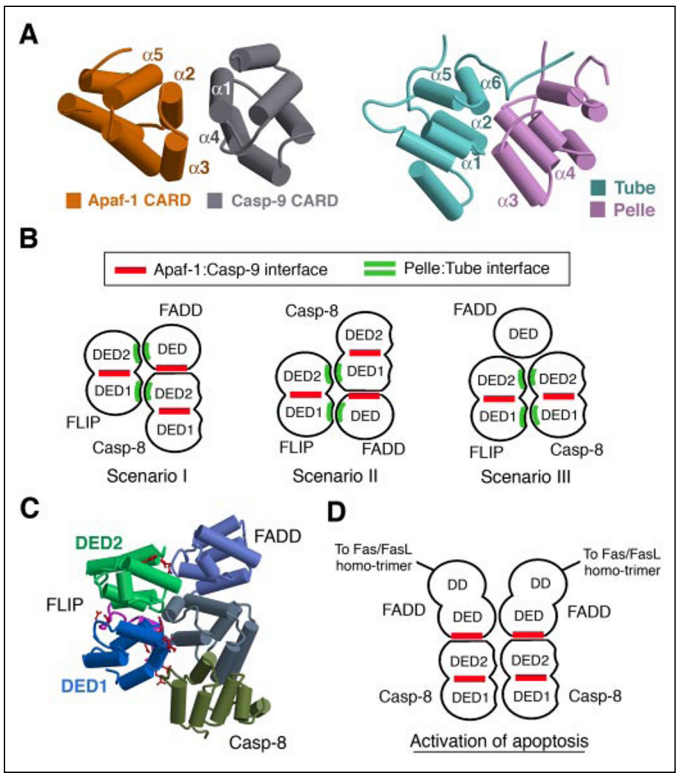

FIGURE 5. **Implications for interactions among FLIP, FADD, and caspase-8.** *A*, two documented modes of interaction for the homotypic interaction motifs. The *left* and *right panels* show the overall domain orientations of the CARD·CARD complex between Apaf-1 and caspase-9 (51) and the DD·DD complex between Pelle and Tube (53). *B*, three hypothetical models on how MC159 may interact with the DED domains of FADD and caspase-8. The models are based on the assumption that the interaction between MC159 and caspase-8 or FADD mimics that between Pelle and Tube. This assumption is supported by mutagenesis studies (52) as well as the surface locations of the binding elements on MC159. *C*, a detailed atomic model for scenario I of the proposed models in *panel B*. The amino acids whose mutations contribute to loss-of-function are highlighted in *red*. Note that most of these residues are predicted by this model to participate in binding to caspase-8 and FADD. *D*, a speculative model on the assembly of DISC. In this model, caspase-8 and FADD have additional interactions among themselves, which allow oligomerization of the trimerized receptor complexes. Viral FLIPs and c-FLIP$_S$ can disrupt these interactions, thus blocking the activation of caspase-8.

CONCLUSION

The structure of the v-FLIP MC159 reveals two unexpected findings. First, the two tandem DED domains of MC159 are held together by conserved and predominantly hydrophobic interactions. Structural and sequence analyses indicate that the structure of MC159, including the DED1-DED2 interface, is representative of all other tandem DED-containing proteins. Second, the relative orientation of the two DED domains in MC159 closely resembles that of the CARD·CARD complex between Apaf-1 and caspase-9. The structure of MC159 also allows us to interpret previous mutagenesis studies. Such analysis revealed two additional findings. First, each DED domain of MC159 contains a conserved binding element on the surface, which is poised for binding to other protein(s). Structural and sequence analyses indicate that this binding element is highly conserved in other tandem DED-containing proteins. Second, this conserved binding element corresponds to the region in the DED of PEA-15, which is required for binding to its partner kinase, and the region in the DD of Tube, which is required for binding to the DD of Pelle. The recurring patterns of relative domain orientation among the homotypic interaction motifs allow us to propose speculative models to explain the function of FLIPs. Future experiments should be directed to structure-guided biological investigation and structure determination of complexes between MC159 and its interacting proteins.

Acknowledgments—We thank Jeffrey Cohen (NIAID, National Institutes of Health) for the MC159 cDNA, Matthew Neiditch for sharing his synchrotron time at the NSLS X25 beamline, and members of the Shi laboratory for helpful discussions.

REFERENCES

1. Horvitz, H. R. (2003) *Chembiochem* **4,** 697–711
2. Danial, N. N., and Korsmeyer, S. J. (2004) *Cell* **116,** 205–219
3. Wang, X. (2001) *Genes Dev.* **15,** 2922–2933
4. Hay, B. A., Huh, J. R., and Guo, M. (2004) *Nat. Rev. Genet.* **5,** 911–922
5. Rathmell, J. C., and Thompson, C. B. (2002) *Cell* **109,** S97–S107
6. Thompson, C. B. (1995) *Science* **267,** 1456–1462
7. Hanahan, D., and Weinberg, R. A. (2000) *Cell* **100,** 57–70
8. Yuan, J., and Yankner, B. A. (2000) *Nature* **407,** 802–809
9. Green, D. R., and Evan, G. I. (2002) *Cancer Cell* **1,** 19–30
10. Vaux, D. L., and Flavell, R. A. (2000) *Curr. Opin. Immunol.* **12,** 719–724
11. Riedl, S. J., and Shi, Y. (2004) *Nat. Rev. Mol. Cell. Biol.* **5,** 897–907
12. Thornberry, N. A., and Lazebnik, Y. (1998) *Science* **281,** 1312–1316
13. Nagata, S. (1999) *Annu. Rev. Genet.* **33,** 29–55
14. Peter, M. E., and Krammer, P. H. (2003) *Cell Death Differ.* **10,** 26–35
15. Ozoren, N., and El-Deiry, W. S. (2003) *Semin. Cancer Biol.* **13,** 135–147
16. Holler, N., Tardivel, A., Kovacsovics-Bankowski, M., Hertig, S., Gaide, O., Martinon, F., Tinel, A., Deperthes, D., Calderara, S., Schulthess, T., Engel, J., Schneider, P., and Tschopp, J. (2003) *Mol. Cell. Biol.* **23,** 1428–1440
17. Boldin, M. P., Varfolomeev, E. E., Pancer, Z., Mett, I. L., Camonis, J. H., and Wallach, D. (1995) *J. Biol. Chem.* **270,** 7795–7798
18. Chinnaiyan, A. M., O'Rourke, K., Tewari, M., and Dixit, V. M. (1995) *Cell* **81,** 505–512
19. Kischkel, F. C., Lawrence, D. A., Tinel, A., LeBlanc, H., Virmani, A., Schow, P., Gazdar, A., Blenis, J., Arnott, D., and Ashkenazi, A. (2001) *J. Biol. Chem.* **276,** 46639–46646
20. Muzio, M., Chinnaiyan, A. M., Kischkel, F. C., O'Rourke, K., Shevchenko, A., Ni, J., Scaffidi, C., Bretz, J. D., Zhang, M., Gentz, R., Mann, M., Krammer, P. H., Peter, M. E., and Dixit, V. M. (1996) *Cell* **85,** 817–827
21. Wang, J., Chun, H. J., Wong, W., Spencer, D. M., and Lenardo, M. J. (2001) *Proc. Natl. Acad. Sci. U. S. A.* **98,** 13884–13888
22. Thome, M., and Tschopp, J. (2001) *Nat. Rev. Immunol.* **1,** 50–58
23. Bertin, J., Armstrong, R. C., Ottilie, S., Martin, D. A., Wang, Y., Banks, S., Wang, G. H., Senkevich, T. G., Alnemri, E. S., Moss, B., Lenardo, M. J., Tomaselli, K. J., and Cohen, J. I. (1997) *Proc. Natl. Acad. Sci. U. S. A.* **94,** 1172–1176
24. Hu, S., Vincenz, C., Buller, M., and Dixit, V. M. (1997) *J. Biol. Chem.* **272,** 9621–9624
25. Thome, M., Schneider, P., Hofmann, K., Fickenscher, H., Meinl, E., Neipel, F., Mattmann, C., Burns, K., Bodmer, J. L., Schroter, M., Scaffidi, C., Krammer, P. H., Peter, M. E., and Tschopp, J. (1997) *Nature* **386,** 517–521
26. Wang, G. H., Bertin, J., Wang, Y., Martin, D. A., Wang, J., Tomaselli, K. J., Armstrong, R. C., and Cohen, J. I. (1997) *J. Virol.* **71,** 8928–8932
27. Djerbi, M., Screpanti, V., Catrina, A. I., Bogen, B., Biberfeld, P., and Grandien, A. (1999) *J. Exp. Med.* **190,** 1025–1032
28. Shisler, J. L., and Moss, B. (2001) *Virology* **282,** 14–25
29. Chang, D. W., Xing, Z., Pan, Y., Algeciras-Schimnich, A., Barnhart, B. C., Yaish-Ohad, S., Peter, M. E., and Yang, X. (2002) *EMBO J.* **21,** 3704–3714
30. Rasper, D. M., Vaillancourt, J. P., Hadano, S., Houtzager, V. M., Seiden, I., Keen, S. L., Tawa, P., Xanthoudakis, S., Nasir, J., Martindale, D., Koop, B. F., Peterson, E. P., Thornberry, N. A., Huang, J., MacPherson, D. P., Black, S. C., Hornung, F., Lenardo, M. J., Hayden, M. R., Roy, S., and Nicholson, D. W. (1998) *Cell Death Differ* **5,** 271–288
31. Shu, H. B., Halpin, D. R., and Goeddel, D. V. (1997) *Immunity* **6,** 751–763
32. Nicholls, A., Sharp, K. A., and Honig, B. (1991) *Proteins: Struct. Funct. Genet.* **11,** 281–296
33. Srinivasula, S. M., Ahmad, M., Ottilie, S., Bullrich, F., Banks, S., Wang, Y., Fernandes-Alnemri, T., Croce, C. M., Litwack, G., Tomaselli, K. J., Armstrong, R. C., and Alnemri, E. S. (1997) *J. Biol. Chem.* **272,** 18542–18545
34. Inohara, N., Koseki, T., Hu, Y., Chen, S., and Nunez, G. (1997) *Proc. Natl. Acad. Sci. U. S. A.* **94,** 10717–10722
35. Irmler, M., Thome, M., Hahne, M., Schneider, P., Hofmann, K., Steiner, V., Bodmer, J. L., Schroter, M., Burns, K., Mattmann, C., Rimoldi, D., French, L. E., and Tschopp, J. (1997) *Nature* **388,** 190–195
36. Han, D. K., Chaudhary, P. M., Wright, M. E., Friedman, C., Trask, B. J., Riedel, R. T., Baskin, D. G., Schwartz, S. M., and Hood, L. (1997) *Proc. Natl. Acad. Sci. U. S. A.* **94,** 11333–11338
37. Eberstadt, M., Huang, B., Chen, Z., Meadows, R. P., Ng, S.-C., Zheng, L., Lenardo, M. J., and Fesik, S. W. (1998) *Nature* **392,** 941–945
38. Hill, J. M., Vaidyanathan, H., Ramos, J. W., Ginsberg, M. H., and Werner, M. H. (2002) *EMBO J.* **21,** 6494–6504
39. Huang, B., Eberstadt, M., Olejniczak, E. T., Meadows, R. P., and Fesik, S. W. (1996)

Nature **384,** 638–641
40. Berglund, H., Olerenshaw, D., Sankar, A., Federwisch, M., McDonald, N. Q., and Driscoll, P. C. (2000) *J. Mol. Biol.* **302,** 171–188
41. Jeong, E. J., Bang, S., Lee, T. H., Park, Y. I., Sim, W. S., and Kim, K. S. (1999) *J. Biol. Chem.* **274,** 16337–16342
42. Fesik, S. W. (2000) *Cell* **103,** 273–282
43. Chai, J., Shiozaki, E., Srinivasula, S. M., Wu, Q., Datta, P., Alnemri, E. S., and Shi, Y. (2001) *Cell* **104,** 769–780
44. Li, W., Srinivasula, S. M., Chai, J., Li, P., Wu, J.-W., Zhang, Z., Alnemri, E. S., and Shi, Y. (2002) *Nat. Struct. Biol.* **9,** 436–441
45. Otwinowski, Z., and Minor, W. (1997) *Methods Enzymol.* **276,** 307–326
46. Sheldrick, G. M. (1990) *Acta Crystallogr. Sect. A* **46,** 467–473
47. Perrakis, A., Morris, R., and Lamzin, V. S. (1999) *Nat. Struct. Biol.* **6,** 458–463
48. Jones, T. A., Zou, J.-Y., Cowan, S. W., and Kjeldgaard, M. (1991) *Acta Crystallogr. A* **47,** 110–119
49. Brunger, A. T., Adams, P. D., Clore, G. M., Delano, W. L., Gros, P., Grosse-Kunstleve, R. W., Jiang, J. S., Kuszewski, J., Nilges, M., Pannu, N. S., Read, R. J., Rice, L. M., Simonson, T., and Warren, G. L. (1998) *Acta Crystallogr. Sect. D Biol. Crystallogr.* **54,** 905–921
50. Holm, L., and Sander, C. (1993) *J. Mol. Biol.* **233,** 123–138
51. Qin, H., Srinivasula, S. M., Wu, G., Fernandes-Alnemri, T., Alnemri, E. S., and Shi, Y. (1999) *Nature* **399,** 547–555
52. Garvey, T. L., Bertin, J., Siegel, R. M., Wang, G. H., Lenardo, M. J., and Cohen, J. I. (2002) *J. Virol.* **76,** 697–706
53. Xiao, T., Towb, P., Wasserman, S. A., and Sprang, S. R. (1999) *Cell* **99,** 545–555
54. Siegel, R. M., Martin, D. A., Zheng, L., Ng, S. Y., Bertin, J., Cohen, J., and Lenardo, M. J. (1998) *J. Cell Biol.* **141,** 1243–1253
55. Kraulis, P. J. (1991) *J. Appl. Crystallogr.* **24,** 946–950